JOURNAL OF AIRCRAFT
Vol. 40, No. 4, July–August 2003

Active Control of Gimballed Rotors Using Swashplate Actuation During Shipboard Engagement Operations

Jonathan A. Keller* and Edward C. Smith†
The Pennsylvania State University, University Park, Pennsylvania 16802-1401

An analysis has been developed to investigate the feedback control of gimballed rotor systems using swashplate actuation during transient shipboard engagement operations. The equations of motion for a rigid, three-bladed gimballed rotor system were derived using a Newtonian force summation method. Aerodynamic forces were simulated with a blade-element linear attached flow model. The resulting equations of motion were time integrated along a specified rotor-speed profile. A time domain linear-quadratic-regulator optimal control technique was applied to the equations of motion to minimize the transient rotor response. The physical limits of collective and cyclic pitch inputs in both magnitude and rate were enforced. The maximum transient gimbal tilt angle was reduced by as much as 56% with full knowledge of the ship air-wake environment and 42% with only partial knowledge of the ship airwake environment. Increasing the physical limits of collective and cyclic pitch inputs achieved up to a 70% reduction in the maximum transient gimbal tilt angle.

Nomenclature

$\boldsymbol{A}$	=	state matrix
$\boldsymbol{B}$	=	control matrix
$\boldsymbol{C}$	=	damping matrix
C_{l_α}	=	two-dimensional lift curve slope
c	=	blade chord
$\boldsymbol{d}$	=	disturbance vector
$\boldsymbol{F}$	=	force vector
F_z	=	vertical aerodynamic force
g	=	gravity
$\boldsymbol{I}$	=	identity matrix
I_b	=	blade second mass moment of inertia
J	=	quadratic performance index
$\boldsymbol{K}$	=	stiffness matrix
$\boldsymbol{K}_G$	=	Kalman gain matrix
K_β	=	hub spring stiffness
$k_{p\beta}$	=	pitch-flap coupling parameter
$\boldsymbol{M}$	=	mass matrix
M_{A_x}, M_{A_y}	=	aerodynamic moments
M_i	=	blade-root flapping moment
N_b	=	number of blades
$\boldsymbol{Q}$	=	state weighting matrix
R	=	blade radius
$\boldsymbol{R}$	=	control-effort weighting matrix
r	=	radial coordinate
$\boldsymbol{S}$	=	final-state weighting matrix
S_b	=	blade first mass moment of inertia
$\boldsymbol{T}_{\text{ac}}$	=	control system-actuator transformation matrix
t	=	time
t_f	=	final time
U_T, U_P	=	blade section velocities
$\boldsymbol{u}$	=	control vector
V_{WOD}	=	wind-over-deck velocity
$\forall_x, \forall_y, \forall_z$	=	mean ship air-wake velocities
$\boldsymbol{v}$	=	bias vector
$\boldsymbol{x}$	=	state vector
$\boldsymbol{x}_{\text{ac}}$	=	actuator displacement vector
β_i	=	blade flap angle
$\beta_{\max}$	=	rotor maximum gimbal tilt angle
β_p	=	blade precone angle
β_{1c}, β_{1s}	=	lateral and longitudinal cyclic flap angles
θ_{tw}	=	effective blade twist
θ_0	=	total blade section pitch angle
$\theta_{75}, \theta_{1c}, \theta_{1s}$	=	collective, lateral, and longitudinal cyclic pitch inputs
ρ	=	air density
ψ_i	=	blade azimuth angle
ψ_{WOD}	=	wind-over-deck direction
Ω	=	time-varying rotor speed
Ω_0	=	full rotor speed
$()_A$	=	aerodynamic contribution
$()_E$	=	error contribution
$()_S$	=	structural contribution
$(\cdot)$	=	$\partial/\partial t$

Introduction

AT the beginning of every helicopter mission, the rotor must be accelerated from rest to full rotor speed and vice versa at the end of every mission. This process is called the engagement and disengagement of the rotor system. It is normally a very mundane procedure when conducted in calm winds; however, when conducted in an unusual flow pattern, such as that encountered near a building or hangar, the rotor blades can occasionally generate appreciable aerodynamic forces. Combined with low rotor speed and low centrifugal stiffening, excessive amounts of aeroelastic flapping can occur. This problem occurs most often in a maritime environment. For articulated and hingeless rotors, which utilize relatively flexible blades, potential contact between the blades and the fuselage is the primary concern. For gimballed tiltrotors, which utilize relatively stiff blades, contact between the blades and the fuselage is quite unlikely; however, impacts between the hub and the restraint mechanism are still possible. In this case excessive transient loads in the blades and pylon are the primary concern.

Previous engagement and disengagement research has been conducted at the University of Southampton,[1–6] Penn State

Received 15 February 2002; revision received 7 October 2002; accepted for publication 15 March 2003.

*Rotorcraft Fellow; currently Aerospace Engineer, U.S. Army AMCOM, Attn: AMSAM-RD-AE-A, Building 4488, Room B-377, Redstone Arsenal, Alabama 35898-5000. Member AIAA.

†Associate Professor, Department of Aerospace Engineering, 233 Hammond Building. Member AIAA.

University,[7–9] McDonnell Douglas,[10] and Georgia Tech.[11] Primarily, this research has been focused on the prediction of the transient blade behavior and loads in various airwake conditions. Initial research into the control of the transient blade behavior using several passive methods has been completed at Penn State University.[12–14] To date, little research has been conducted using active control techniques.

Objectives

In this paper an analytic feasibility study is conducted to determine the effectiveness of using a time-domain active control system during the engagement of a gimballed rotor to reduce the transient gimbal tilt angle. The proposed time-domain controller uses feedback from the measured blade motion to actuate the primary control system inputs. The effectiveness and robustness of the controller in different air-wake conditions will be assessed. In addition, the effect of the physical limits of the control system will be examined.

Approach

In this section an abbreviated derivation of the equations of motion for a rigid, gimballed rotor is presented. A full derivation is presented in Ref. 14. Compared to most articulated rotor blades, gimballed rotor blades are relatively short and stiff. In addition, the blades are rigidly attached to each other through the rotor hub and pivot as a rigid body about a universal joint. The majority of the cyclic flapping motion is caused by the rigid-body motion of the entire rotor system about the hub, not the elastic motion of the blades. Therefore, a rigid blade assumption is more justified for a gimballed rotor than for an articulated rotor for the current analysis. A schematic of the gimballed rotor is shown in Fig. 1.

The individual blade flapping moment about the hub is given by

$$M_i = -I_b\ddot{\beta}_i - I_b\Omega(t)^2\beta_i + \int_0^R F_z r\,\mathrm{d}r - S_b g \tag{1}$$

The individual blade flap angle can be written in terms of the fixed-frame flap angles as

$$\beta_i = \beta_P + \beta_{1c}\cos\psi_i(t) + \beta_{1s}\sin\psi_i(t) \tag{2}$$

Summing the individual blade moments about the rotor hub yields

$$\sum_{i=1}^{N_b} M_i\cos\psi_i(t) = K_\beta\beta_{1c}$$

$$\sum_{i=1}^{N_b} M_i\sin\psi_i(t) = K_\beta\beta_{1s} \tag{3}$$

The individual blade equations of motion are then transferred into two rotor equations of motion for the fixed frame degrees of freedom. Premultiplication of all remaining terms by $2/N_b$ and nondimensionalizing by $I_b\Omega_0^2$ yields

$$\boldsymbol{M}_s\begin{Bmatrix}\ddot{\beta}_{1c}\\ \ddot{\beta}_{1s}\end{Bmatrix} + \boldsymbol{C}_s\begin{Bmatrix}\dot{\beta}_{1c}\\ \dot{\beta}_{1s}\end{Bmatrix} + \boldsymbol{K}_s\begin{Bmatrix}\beta_{1c}\\ \beta_{1s}\end{Bmatrix} = \begin{Bmatrix}M_{A_x}\\ M_{A_y}\end{Bmatrix} \tag{4}$$

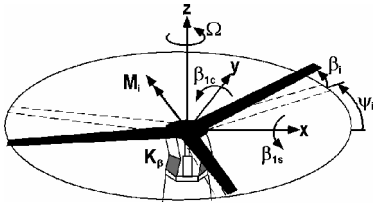

Fig. 1 Gimballed rotor schematic.

The structural mass, damping, and stiffness matrices are given by

$$\boldsymbol{M}_s = \begin{bmatrix}1 & 0\\ 0 & 1\end{bmatrix}, \qquad \boldsymbol{C}_s = 2\frac{\Omega(t)}{\Omega_0}\begin{bmatrix}0 & 1\\ -1 & 0\end{bmatrix}$$

$$\boldsymbol{K}_s = \begin{bmatrix}\dfrac{2K_\beta}{N_b I_b\Omega_0^2} & \dfrac{\Omega(t)}{\Omega_0^2}\\ \dfrac{-\Omega(t)}{\Omega_0^2} & \dfrac{2K_\beta}{N_b I_b\Omega_0^2}\end{bmatrix} \tag{5}$$

The aerodynamic moments about the rotor hub are assumed to consist of contributions from the vertical aerodynamic force only. Blade-section aerodynamic pitching moments are not included. The aerodynamic moments are then approximated by

$$\begin{Bmatrix}M_{A_x}\\ M_{A_y}\end{Bmatrix} \approx \frac{2}{N_b I_b\Omega_0^2}\begin{Bmatrix}\displaystyle\sum_{i=1}^{N_b}\int_0^R F_z r\,\mathrm{d}r\cos\psi_i(t)\\ \displaystyle\sum_{i=1}^{N_b}\int_0^R F_z r\,\mathrm{d}r\sin\psi_i(t)\end{Bmatrix} \tag{6}$$

For this analytic feasibility study the vertical aerodynamic force is derived using a two-dimensional, quasi-steady, linear aerodynamic model and is approximated by

$$F_z \approx \tfrac{1}{2}\rho c C_{l_\alpha}\left(\theta_0 U_T^2 - U_P U_T\right) \tag{7}$$

The total blade pitch angle is a function of the control system inputs, built-in twist, and the pitch-flap coupling

$$\theta_0 = \theta_{75} + \theta_{1c}\cos\psi_i(t) + \theta_{1s}\sin\psi_i(t) + \theta_{\mathrm{tw}}\left(r/R - \tfrac{3}{4}\right) - k_{p\beta}(\beta_i - \beta_p) \tag{8}$$

The blade-section velocities in the shaft plane are given by

$$U_T = \Omega r + \forall_x\sin\psi_i + \forall_y\cos\psi_i$$

$$U_P = r\dot{\beta}_i + (\forall_x\cos\psi_i - \forall_y\sin\psi_i)\beta_i - \forall_z \tag{9}$$

In this analytic study the mean ship air-wake velocities are defined using simple deterministic expressions, derived from model-scale measurements correlated with limited full-scale measurements.[1] The constant and linear air-wake distributions, shown in Fig. 2, are examined in this study. The in plane mean ship air-wake velocities for both distributions are defined as

$$\forall_x = V_{\mathrm{WOD}}\cos\psi_{\mathrm{WOD}}, \qquad \forall_y = -V_{\mathrm{WOD}}\sin\psi_{\mathrm{WOD}} \tag{10}$$

The constant and linear air-wake distributions are differentiated by the out-of-plane mean ship air-wake velocity, which is given by

$$\forall_z = \begin{cases}\kappa V_{\mathrm{WOD}} & \text{constant}\\ \kappa V_{\mathrm{WOD}}(r/R)\sin[\psi_i - (\pi/2 - \psi_{\mathrm{WOD}})] & \text{linear}\end{cases} \tag{11}$$

where κ defines the maximum out-of-plane mean ship air-wake velocity in terms of the wind-over-deck speed. Substitution of Eqs. (7–11) into Eq. (6) yields

$$\begin{Bmatrix}M_{A_x}\\ M_{A_y}\end{Bmatrix} = -\boldsymbol{C}_A\begin{Bmatrix}\dot{\beta}_{1c}\\ \dot{\beta}_{1s}\end{Bmatrix} - \boldsymbol{K}_A\begin{Bmatrix}\beta_{1c}\\ \beta_{1s}\end{Bmatrix} + \boldsymbol{F}_A \tag{12}$$

The aerodynamic damping and stiffness matrices and force vector are dependent upon the number of blades and the air-wake distribution and are given in Ref. 14. Combining like terms in Eqs. (4) and (12) yields

$$\boldsymbol{M}\begin{Bmatrix}\ddot{\beta}_{1c}\\ \ddot{\beta}_{1s}\end{Bmatrix} + \boldsymbol{C}\begin{Bmatrix}\dot{\beta}_{1c}\\ \dot{\beta}_{1s}\end{Bmatrix} + \boldsymbol{K}\begin{Bmatrix}\beta_{1c}\\ \beta_{1s}\end{Bmatrix} = \boldsymbol{F} \tag{13}$$

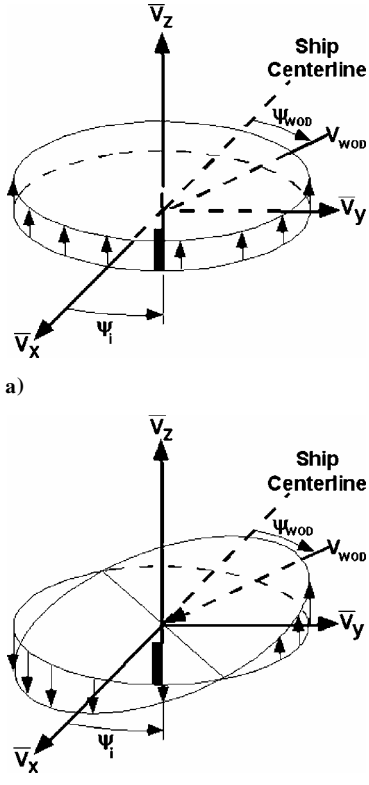

Fig. 2 Schematic of a) constant and b) linear air-wake distributions.

Optimal Control Theory

The final equations of motion are then transferred into state-space form. Because the rotor acceleration, speed, and azimuth angles are nonperiodic functions of time, the resulting state-space equations are linear time variant

$$\dot{\boldsymbol{x}} = \boldsymbol{A}(t)\boldsymbol{x} + \boldsymbol{B}(t)\boldsymbol{u} + \boldsymbol{d}(t) \tag{14}$$

The state vector and input vector are defined as

$$\boldsymbol{x} = \{\beta_{1c} \;\; \beta_{1s} \;\; \dot{\beta}_{1c} \;\; \dot{\beta}_{1s}\}^T, \qquad \boldsymbol{u} = \{\theta_{75} \;\; \theta_{1c} \;\; \theta_{1s}\}^T \tag{15}$$

Note that there is an additional term $\boldsymbol{d}$ in the state equation. Typically, this term is called the "disturbance" and is often used to represent external noise. That is not the case in the current analysis. Here the disturbance term is a known quantity and arises from aerodynamic forces generated by anything other than the pilot control inputs, such as blade twist and out-of-plane winds.

Because the equations of motion are time variant, traditional frequency domain control approaches, such as pole placement, are ineffective. Instead, a time-domain linear quadratic regulator control method is used.[15] A quadratic performance index is defined as

$$J = \frac{1}{2}\boldsymbol{x}^T(t_f)\boldsymbol{S}(t_f)\boldsymbol{x}(t_f) + \frac{1}{2}\int_0^{t_f} (\boldsymbol{x}^T\boldsymbol{Q}\boldsymbol{x} + \boldsymbol{u}^T\boldsymbol{R}\boldsymbol{u})\,\mathrm{d}t \tag{16}$$

The matrix $\boldsymbol{S}(t_f)$ weights the final state, $\boldsymbol{Q}$ weights the time variation of the state, and $\boldsymbol{R}$ weights the control inputs. These matrices are user specified. The matrices $\boldsymbol{S}$ and $\boldsymbol{Q}$ are symmetric and positive semidefinite, and $\boldsymbol{R}$ is symmetric and positive definite.

Assuming the final state is free, the matrix Ricatti equations (MRE) can then be used to solve for the time variation of $\boldsymbol{S}$:

$$-\dot{\boldsymbol{S}} = \boldsymbol{A}^T\boldsymbol{S} + \boldsymbol{S}\boldsymbol{A} - \boldsymbol{S}\boldsymbol{B}\boldsymbol{R}^{-1}\boldsymbol{B}^T\boldsymbol{S} + \boldsymbol{Q} \tag{17}$$

Given $\boldsymbol{S}(t_f)$, the MRE are then solved backward in time for $\boldsymbol{S}$. The Kalman gain matrix is then given by

$$\boldsymbol{K}_G = \boldsymbol{R}^{-1}\boldsymbol{B}^T\boldsymbol{S} \tag{18}$$

Because the weighting matrix $\boldsymbol{S}$ varies in time, then so does the Kalman gain matrix. Because of the disturbance term in the state equation, an additional time-varying bias term exists in the MRE. The time variation of the bias term is given by

$$-\dot{\boldsymbol{v}} = (\boldsymbol{A} - \boldsymbol{B}\boldsymbol{K}_G)^T\boldsymbol{v} + \boldsymbol{S}\boldsymbol{d} \tag{19}$$

where $\boldsymbol{v}(t_f)$ is zero. This equation is also solved backward in time for $\boldsymbol{v}$. The closed-loop optimal control vector is then given by

$$\boldsymbol{u} = -\boldsymbol{K}_G\boldsymbol{x} - \boldsymbol{R}^{-1}\boldsymbol{B}^T\boldsymbol{v} \tag{20}$$

The second term in the equation is caused by the disturbance term. The response of the closed-loop system is then given by

$$\dot{\boldsymbol{x}} = (\boldsymbol{A} - \boldsymbol{B}\boldsymbol{K}_G)\boldsymbol{x} - \boldsymbol{B}\boldsymbol{R}^{-1}\boldsymbol{B}^T\boldsymbol{v} + \boldsymbol{d} \tag{21}$$

Given an initial state, this equation can be integrated forward in time for the optimal state trajectory.

Control System Limits

On modern rotorcraft actuators are used to control the movements of the swashplate and the control system inputs. The relation between the motion of the actuators and the control system inputs is given by

$$\boldsymbol{u} = \boldsymbol{T}_{\mathrm{ac}}\,\boldsymbol{x}_{\mathrm{ac}}, \qquad \dot{\boldsymbol{u}} = \boldsymbol{T}_{\mathrm{ac}}\,\dot{\boldsymbol{x}}_{\mathrm{ac}} \tag{22}$$

Swashplate actuators typically have limits in magnitude and rate. These limits are enforced in the current analysis. In the time integration of the closed-loop response, if any of the calculated optimal control inputs are greater than the maximum allowable control inputs, the maximum allowable control inputs are used. Therefore, this study was not conducted as a constrained optimization problem.

Results

Using the simple analysis outlined in the preceding section, a study is conducted to determine the effectiveness of using feedback from the gimbal tilt angles to the control system inputs to minimize the flapping response of a three-bladed gimballed rotor. The time history of the rotor response and required control system effort will be examined. A useful metric of the rotor response is the maximum tilt angle of the rotor and is expressed as

$$\beta_{\max} = \sqrt{\beta_{1c}^2 + \beta_{1s}^2} \tag{23}$$

The angle at which the hub would contact the gimbal restraint is called β_r. Contact between the gimbal and the restraint is not enforced in this model; however, comparison of the maximum gimbal tilt angle to the gimbal restraint angle provides a useful measure of excessive tilt.

The properties of the gimballed rotor model are loosely based on the V-22 Osprey rotor system and are listed in Table 1. The engagement rotor-speed profile for the gimballed rotor is assumed an offset sine wave, reaching 50%NR in 10 s and full rotor speed in 20 s. As seen in Fig. 3, this assumption approximates the measured rotor-speed profile for a H-46 Sea Knight. The gimballed rotor used in the analysis also has several limits on the allowable control system inputs. It is assumed the collective pitch has a lower limit of −7.5 deg and an upper limit of 54 deg. The lateral cyclic pitch has assumed limits of ±10 deg. Furthermore, it is assumed that each of the linear hydraulic actuators has maximum extension/retraction rate limits of ±7 in./s. The actuator transformation matrix is given by

$$\boldsymbol{T}_{\mathrm{ac}} = \begin{bmatrix} 0.2275 & 0.0 & -0.2627 \\ 0.2275 & 0.2275 & 0.0 \\ 0.2275 & -0.2275 & 0.0 \end{bmatrix} \left(^{\circ}/\mathrm{in}\right) \tag{24}$$

Table 1 Rigid Gimballed Rotor System Properties

Parameter	Value
Number of blades, N_b	3
Mass moment of inertia, I_b	742.6 slug-ft^2
Full rotor speed, Ω_0	397 rpm
Radius, R	19 ft
Gimbal restraint angle, β_r	11 deg
Gimbal spring stiffness, K_β	250 ft-lb/deg
Effective blade twist, θ_{tw}	−47.5
Pitch-flap coupling, $k_{p\beta}$	0.274
Precone, β_p	2.5 deg

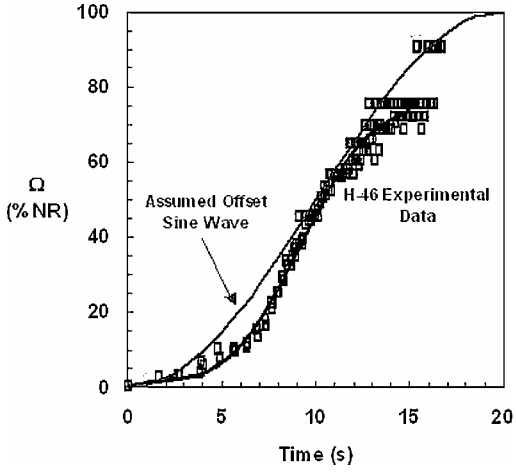

Fig. 3 Rotor-speed profile.

Optimal Control System Results

Rotor engagements were simulated in the constant and linear air-wake distributions in 30-kn bow winds. The response for the uncontrolled rotor system was generated assuming zero control inputs. For the initial analysis the control system weights were set at values of $\boldsymbol{S}(t_f) = 0$, $\boldsymbol{Q} = 4\boldsymbol{I}_4$, and $\boldsymbol{R} = \boldsymbol{I}_3$. No weighting is needed on the final state of the system because the gimbal tilt naturally decreases as the rotor nears full speed and full centrifugal force.

The results in the constant air-wake distribution are shown in Figs. 4a–4c. For the uncontrolled case the rotor would initially be in contact with the gimbal restraint at 11 deg (not enforced in this model). Even at zero rotor speed, enough aerodynamic forces are generated to significantly tilt the rotor. On two other occasions, at $t = 3.2$ and 4 s where the rotor speed is between 6 and 10%NR the rotor would also tilt far enough to contact the restraint. For the optimally controlled rotor the maximum gimbal tilt angle was reduced to 6.4 deg. The controller also automatically adjusted the control inputs to reduce the initial gimbal tilt angle to 5 deg. The lateral cyclic pitch setting stays well within its limits throughout the engagement, but the collective pitch setting just reaches its lower limit of −7.5 deg at $t = 3$ s. The actuator extension rates are also very close to reaching their limits between $t = 2$ and 4 s.

The results in the linear air-wake distribution are shown in Figs. 5a–5c. The maximum gimbal tilt angle is much lower in the linear air-wake distribution than in the constant air-wake distribution. The uncontrolled rotor reaches a maximum gimbal tilt angle of 8.6 deg. For the optimally controlled rotor the maximum gimbal tilt angle has been reduced by 56% to 3.8 deg. All of the control system inputs are well within their limits throughout the engagement. Although the gimbal tilt angle and control system inputs are lower than in the constant air-wake distribution, the actuator extension rates are actually larger. The actuators repeatedly reach their maximum extension rates between $t = 3$ to 6 s. This is a consequence of the nature of the linear air-wake distribution, in which the vertical flow component changes from upward on the windward side of the rotor to downward on the leeward side of the rotor. In this case the actuators are forced to respond with a higher amplitude and speed than in the constant air-wake distribution, where the vertical flow does not change across the rotor disk.

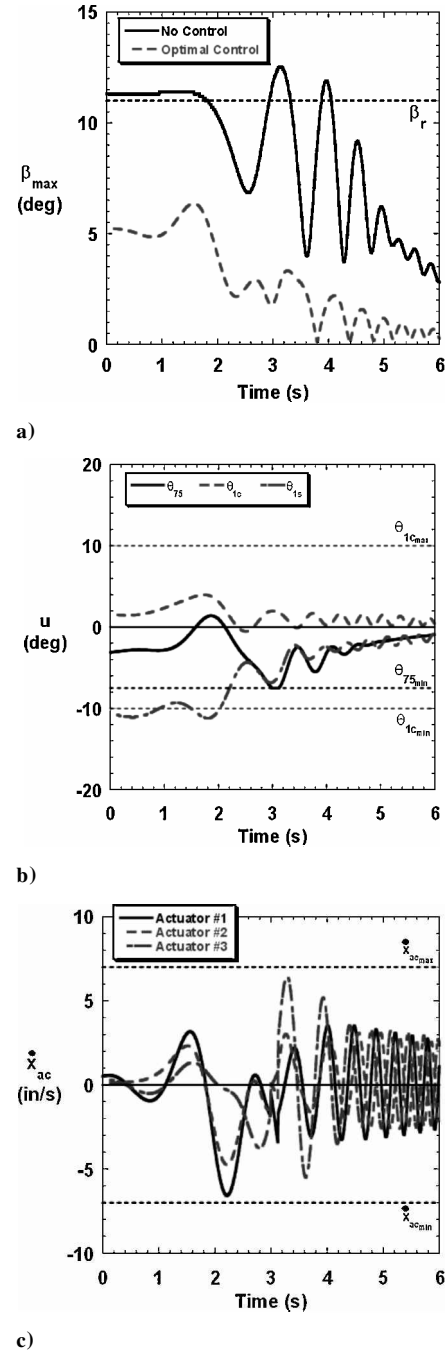

Fig. 4 Time histories of a) maximum gimbal tilt, b) control inputs, and c) actuator extension rates in constant air-wake distribution.

Relaxation of Control System Limits

In the preceding simulations the response of the gimbal was predicted while enforcing the control system limits. In the constant air-wake distribution the minimum collective pitch setting was reached, whereas in the linear air-wake distribution the actuator extension and retraction limits were reached. If the control system limits could be relaxed, the response of the rotor system could be minimized further. This also allows the relative weight of the matrix $\boldsymbol{Q}$ to be increased. In this section the response of the rotor with relaxed control system limits and an increased weight of $\boldsymbol{Q}$ from $4\boldsymbol{I}_4$ to $10\boldsymbol{I}_4$ will be examined.

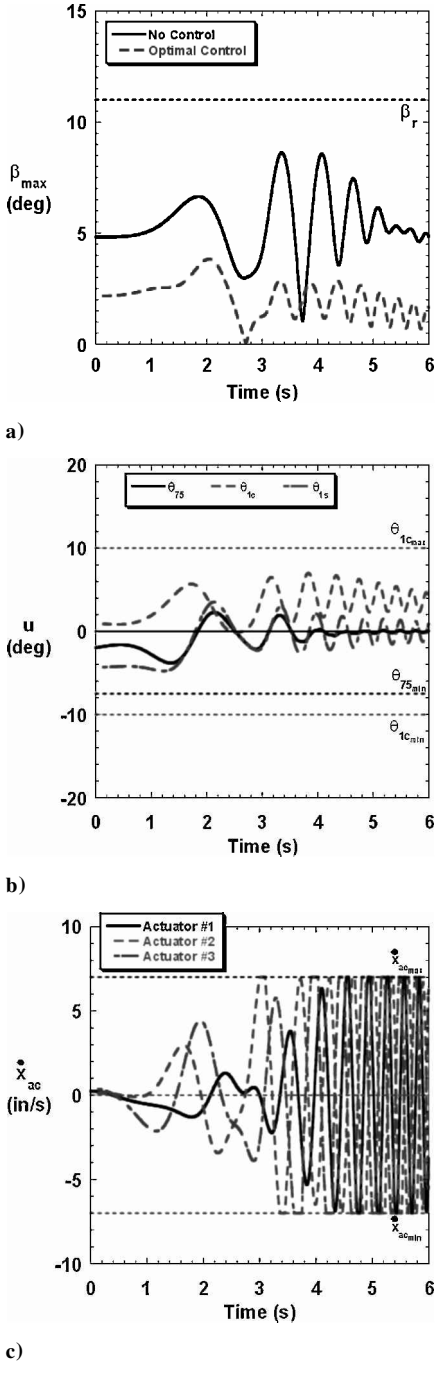

Fig. 5 Time histories of a) maximum gimbal tilt, b) control inputs, and c) actuator extension rates in linear air-wake distribution.

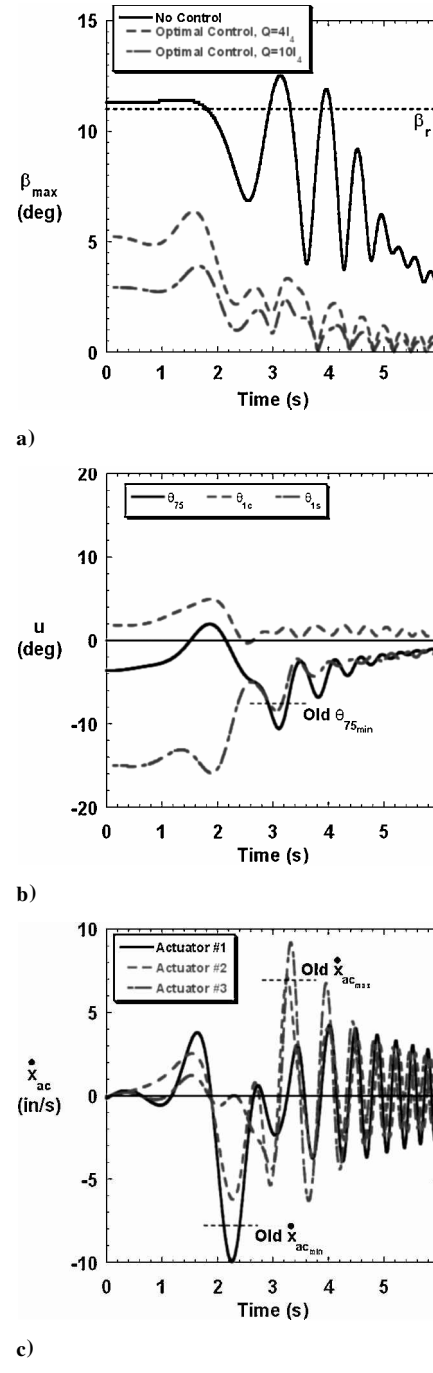

Fig. 6 Time histories of a) maximum gimbal tilt, b) control inputs, and c) actuator extension rates in constant air-wake distribution with relaxed control system limits.

The rotor response in the constant air-wake distribution is shown in Figs. 6a–6c. The maximum gimbal tilt angle has been reduced from 6.4 deg for the original optimal control settings to 3.9 deg with the relaxed control system limits and increased weighting. The original lower limit on the collective pitch setting of -7.5 deg is just briefly exceeded. The largest change is in the actuator extension rates for actuators #1 and #3, which reach nearly ± 10 in./s for brief periods.

The rotor response in the linear air-wake distribution is shown in Figs. 7a–7c. The maximum gimbal tilt angle has been reduced from 3.8 deg for the original optimal control settings to 2.6 deg with the relaxed control system limits. This represents a reduction of 70% compared to the uncontrolled rotor. The actuator extension rates increase to nearly ± 10 in./s between $t = 3$ to 5 s. This coincides with the period in which the largest gimbal tilt angles occur for the uncontrolled rotor.

Suboptimal Control Results

The simulations completed in the preceding sections assumed that the ship air wake in the plane of the rotor disk was completely known. Mathematically, aerodynamic force terms that are largely dependent upon the ship air-wake velocities appear in the $\boldsymbol{A}$, $\boldsymbol{B}$, and $\boldsymbol{d}$ state matrices. These state matrices are then used to calculate the Kalman gain matrix $\boldsymbol{K}_G$ and bias term $\boldsymbol{v}$. Realistically, complete knowledge of the ship air-wake environment is highly unlikely. However, most ships have anemometers that measure the relative wind speed and direction of the oncoming air. As shown schematically in Fig. 8, these anemometers are often located above the flight deck on a mast. The anemometers could be used to obtain an estimate of the wind speeds on the flight deck in the plane of the rotor disk. It is unlikely that an accurate estimate of the out-of-plane wind speed could be made with the ship anemometer. In this section the suboptimal

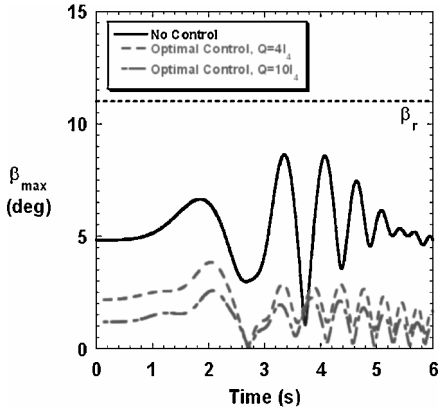

a)

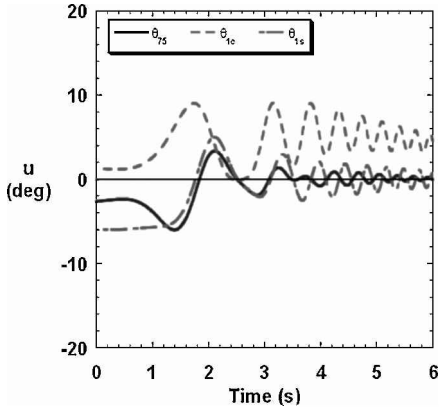

b)

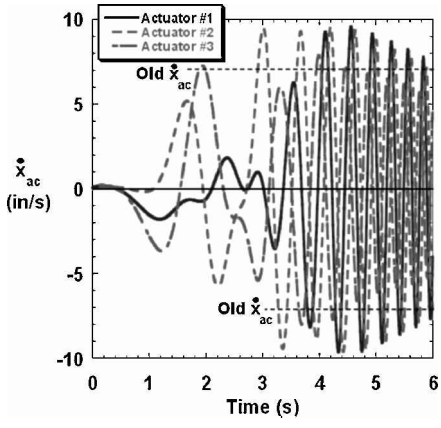

c)

Fig. 7 Time histories of a) maximum gimbal tilt, b) control system inputs, and c) actuator extension rates in linear air-wake distribution with relaxed control system limits.

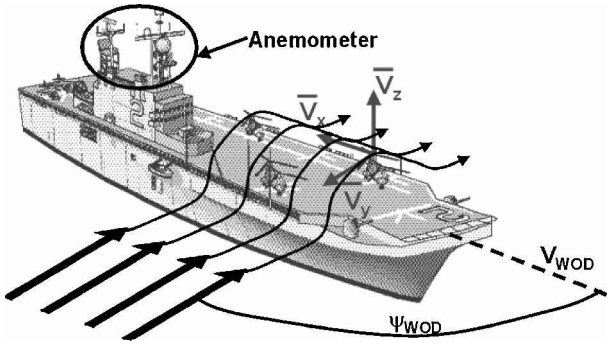

Fig. 8 Ship anemometer schematic.

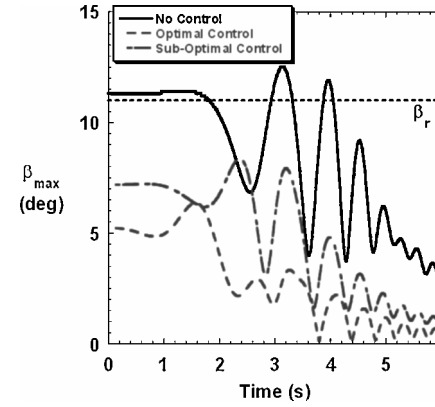

Fig. 9 Time history of maximum gimbal tilt angle in constant air-wake distribution with suboptimal control.

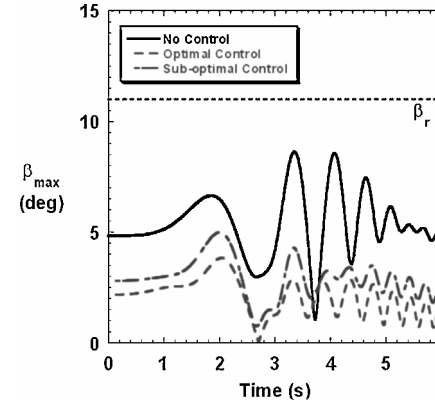

Fig. 10 Time history of maximum gimbal tilt angle in linear air-wake distribution with suboptimal control.

response of the rotor system is investigated. In this context the term suboptimal is used to denote the response of the rotor in which the Kalman gain matrix $\boldsymbol{K}_G$ and bias term $\boldsymbol{v}$ are calculated assuming the in-plane wind speeds are known and the out-of plane wind speed is zero. The original control system weights and limits are used in the investigation.

The response of the rotor system using suboptimal control in the constant air-wake distribution is shown in Fig. 9. The maximum gimbal tilt angle using optimal control is 6.4 deg, whereas the maximum gimbal tilt angle using suboptimal control is 8.4 deg. This still represents a significant reduction from the uncontrolled case. The response of the rotor system using suboptimal control in the linear air-wake distribution is shown in Fig. 10. The uncontrolled rotor reaches a maximum gimbal tilt angle of 8.6 deg. The maximum gimbal tilt angle using optimal control is 3.8 deg, whereas the maximum gimbal tilt angle using suboptimal control is 5 deg, or a reduction of 42% from uncontrolled case.

The ship anemometer might not necessarily give an accurate measure of the ship air-wake velocities on the flight deck. The anemometer is often not physically located near the flight deck, and depending on the ship type the ship airwake over the flight deck might be different than at the anemometer location.

In this section the sensitivity of the suboptimal rotor response to an inaccurate anemometer reading is investigated. It is assumed that the anemometer measurement has some error relative to the actual wind speed and direction on the flight deck. The incorrect information from the anemometer is then used to form incorrect state matrices. These incorrect state matrices are then used to calculate an incorrect Kalman gain matrix and bias vector. The actual response of the rotor is then formed from the true state matrices, but the incorrect optimal

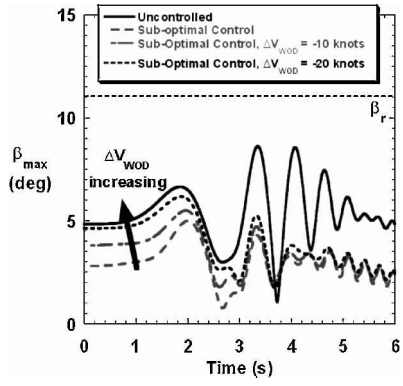

a)

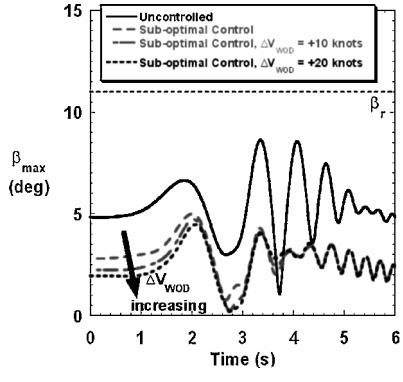

b)

Fig. 11 Time history of maximum gimbal tilt angle in linear air-wake distribution with a) underestimation of wind speed and b) overestimation of wind speed.

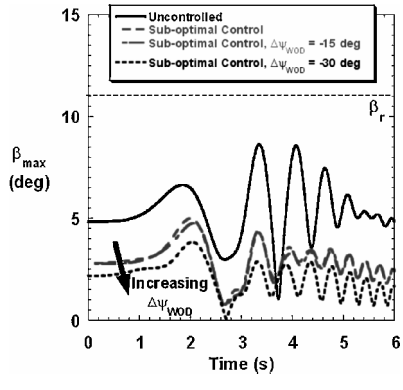

a)

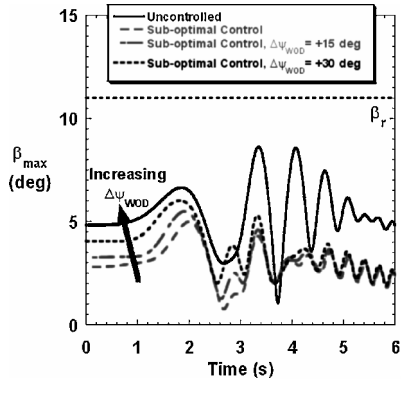

b)

Fig. 12 Time history of maximum gimbal tilt angle in linear air-wake distribution with a) overestimation of wind direction and b) underestimation of wind direction.

control vector

$$\boldsymbol{x}_E = \boldsymbol{A}\boldsymbol{x}_E + \boldsymbol{B}\boldsymbol{u}_E + \boldsymbol{d} \tag{25}$$

The response of the rotor system with an error in the measurement of the wind speed only is shown in Figs. 11a and 11b. In general, the maximum gimbal tilt angle is increased when the wind speed is underestimated and is decreased when the wind speed is overestimated. For a measurement underestimation of 20 kn, the maximum gimbal tilt angle increases from 5 to 6.2 deg. However, this still represents a reduction of 29% from the uncontrolled case. For a measurement overestimation of 20 kn, the maximum gimbal tilt angle actually decreases from 5 to 4.5 deg.

The response of the rotor system with an error in the measurement of the wind direction only is shown in Figs. 12a and 12b. In general, the maximum gimbal tilt angle is decreased when the measured wind direction is more in the counterclockwise direction and increased when the measured wind speed is more in the clockwise direction. For a measurement underestimation of 30 deg, the maximum gimbal tilt angle decreases from 5 to 4.8 deg. For a measurement overestimation of 30 deg, the maximum gimbal tilt angle increases from 5 to 6 deg. However, this still represents a reduction of 30% from the uncontrolled case.

Conclusions

This paper examined the control of the flapping response of a rigid, gimballed rotor system during an engagement operation using feedback from the motion of the rotor to the swashplate actuators. The ship air-wake model was assumed to consist of two different types of deterministic air-wakes, and aerodynamic forces were calculated using a two-dimensional, quasi-steady, linear flow model. A linear-quadratic-regulator optimal control method was used to reduce the flapping of the rotor system. With full knowledge of the ship air-wake velocities, the flapping response of the rotor system was reduced by as much as 56% within the current physical limitations on the control system. If the control limits were relaxed, the flapping response of the rotor was reduced by as much as 70%. With only partial knowledge of the ship air-wake velocities, the flapping response of the rotor system was reduced by as much as 42%. The sensitivity of the rotor response to errors in the ship air-wake measurements was also examined. The rotor response with errors in the ship air-wake measurement of 20 kn and 30 deg was still at least 30% lower than without any control.

Acknowledgments

The authors would like to thank the National Rotorcraft Technology Center for funding this research and the Vertical Flight Foundation for financial assistance. Robert Chen of NASA Ames Research Center, David Miller of Boeing Company, Philadelphia, and David Popelka of Bell Helicopter also provided much technical assistance.

References

[1]Hurst, D. W., and Newman, S. J., "Wind Tunnel Measurements of Ship Induced Turbulence and the Prediction of Helicopter Rotor Blade Response," *Vertica*, Vol. 12, No. 3, 1988, pp. 267–278.

[2]Newman, S. J., "A Theoretical Model for Predicting the Blade Sailing Behaviour of a Semi-Rigid Rotor Helicopter," *Vertica*, Vol. 14, No. 4, 1990, pp. 531–544.

[3]Newman, S. J., "The Application of a Theoretical Blade Sailing Model to Predict the Behaviour of Articulated Helicopter Rotors," *The Aeronautical Journal of the Royal Aeronautical Society*, Vol. 96, No. 956, 1992, pp. 233–239.

[4]Newman, S. J., "The Problems of Rotor Engagement and Disengagement of a Shipborne Helicopter," *Journal of Naval Science*, Vol. 20, No. 1, 1994, pp. 56–64.

[5]Newman, S. J., "The Verification of a Theoretical Helicopter Rotor Blade Sailing Method by Means of Windtunnel Testing," *The Aeronautical Journal of the Royal Aeronautical Society*, Vol. 99, No. 982, 1995, pp. 41–50.

[6]Newman, S. J., "An Investigation into the Phenomenon of Helicopter Blade Sailing," Master's Thesis, Dept. of Aeronautics and Astronautics, Univ. of Southampton, Highfield, Southampton, U.K., March 1995.

[7]Geyer, W. P., Smith, E. C., and Keller, J. A., "Aeroelastic Analysis of Transient Blade Dynamics During Shipboard Engage/Disengage Operations," *Journal of Aircraft*, Vol. 35, No. 3, 1998, pp. 445–453.

[8]Keller, J. A., and Smith, E. C., "An Experimental and Theoretical Correlation of Helicopter Rotor Blade-Droop Stop Impacts," *Journal of Aircraft*, Vol. 36, No. 2, 1999, pp. 443–450.

[9]Kang, H., and Smith, E. C., "Transient Response Analysis of Gimballed Tiltrotors During Engage and Disengage Operations," AIAA Paper 98-2007, April 1998.

[10]Kunz, D. L., "Influence of Elastomeric Damper Modeling on the Dynamic Response of Helicopter Rotors," *AIAA Journal*, Vol. 35, No. 2, 1997, pp. 349–354.

[11]Bottasso, C. L., and Bauchau, O. A., "Multibody Modeling of Engage and Disengage Operations of Helicopter Rotors," *Journal of the American Helicopter Society*, Vol. 46, No. 4, 2001, pp. 290–300.

[12]Keller, J. A., and Smith, E. C., "Analysis and Control of the Transient Shipboard Engagement Behavior of Rotor Systems," *Proceedings of the 55th Annual National Forum of the American Helicopter Society*, American Helicopter Society, Alexandria, VA, 1999, pp. 1064–1078.

[13]Keller, J. A., and Smith, E. C., "Control of the Transient Aeroelastic Response of Rotors During Shipboard Engagement Operations," *Proceedings of the American Helicopter Society Aeromechanics Specialists Meeting*, American Helicopter Society, Alexandria, VA, 2000, pp. 1–16.

[14]Keller, J. A., "Analysis and Control of the Transient Aeroelastic Response of Rotors During Shipboard Engagement and Disengagement Operations," Master's Thesis, Dept. of Aerospace Engineering, Pennsylvania State University, Univ. Park, PA, May 2001, URL: http://etda.libraries.psu.edu/theses/available/etd-0406101-102551/unrestricted/thesis.pdf [cited 1 Oct. 2002].

[15]Lewis, F. L., and Syrmos, V. L., *Optimal Control*, 2nd ed., Wiley, New York, 1995, pp. 161–221.